Damage detection for beam structures based on local flexibility method and macro-strain measurement

Ting Yu Hsu[*1,3], Wen I Liao[2a] and Shen Yau Hsiao[3b]

[1]*Department of Civil and Construction Engineering, National Taiwan University of Science and Technology, Taipei, Taiwan*
[2]*Department of Civil and Environment Engineering, National Taipei University of Technology, Taipei, Taiwan*
[3]*National Center for Research on Earthquake Engineering, Taipei, Taiwan*

Abstract.   Many vibration-based global damage detection methods attempt to extract modal parameters from vibration signals as the main structural features to detect damage. The local flexibility method is one promising method that requires only the first few fundamental modes to detect not only the location but also the extent of damage. Generally, the mode shapes in the lateral degree of freedom are extracted from lateral vibration signals and then used to detect damage for a beam structure. In this study, a new approach which employs the mode shapes in the rotary degree of freedom obtained from the macro-strain vibration signals to detect damage of a beam structure is proposed. In order to facilitate the application of mode shapes in the rotary degree of freedom for beam structures, the local flexibility method is modified and utilized. The proposed rotary approach is verified by numerical and experimental studies of simply supported beams. The results illustrate potential feasibility of the proposed new idea. Compared to the method that uses lateral measurements, the proposed rotary approach seems more robust to noise in the numerical cases considered. The sensor configuration could also be more flexible and customized for a beam structure. Primarily, the proposed approach seems more sensitive to damage when the damage is close to the supports of simply supported beams.

Keywords: local flexibility method; macro-strain; long gauge; beam structure; damage detection

1. Introduction

Vibration-based techniques that detect damage in a structure from changes in global dynamic properties are part of a promising field in structural damage detection. Related structural damage detection researches have attracted much attention in recent years and many approaches have been developed (Johnson et al. 2004). Toksoy and Aktan (1994) first tried to detect damage locations based on structural flexibility matrices of a beam structure; however, their damage detection algorithm lacks a solid theoretical background. Bernal (2002) developed the damage location vector method with a solid theoretical background to determine damage locations of a structure. Reynders and De Roeck (2010) further developed the Local Flexibility Method (LFM) with a robust theoretical background to not only detect damage locations but also the extent of damage. The LFM utilizes flexibility matrices constructed based on mode shapes in the lateral degree of freedom (DOF) before and after damage of a beam structure. Combined with corresponding lateral load configurations that cause strain

and stress fields within a local region of a beam structure, the extent of damage of the local region can be estimated.

Recently, Abdo and Hori (2002) demonstrated the usefulness of the rotation of mode shape as a more sensitive diagnostic parameter than the displacement mode shape for damage localization in flexural structures. However, the application of the rotation of mode shape is restricted to only numerical cases, possibly due to the difficulty in measuring dynamic rotary vibration signals. On the other hand, although most FBG sensors act as localized gauge for point strain measurements (Wan *et al.* 2002, Yung *et al.* 2004, Matthys and Taerwe 2005, Cardini and DeWolf 2009, Wang and Yim 2010, Ni *et al.* 2012, Wang *et al.* 2014), long-gauge strain sensors (Fan *et al.* 1998, Ansari 2005) has illustrated the accuracy and advantage to measure structural response for application to structural health monitoring. Li and Wu (2007) further illustrated the feasibility of damage detection algorithms on the basis of dynamic macro-strain measurements from long-gauge Fiber Bragg grating (FBG) sensors. They also performed parametric estimation of reinforced concrete flexural members using distributed long-gauge FBG sensors (Li and Wu 2010). Therefore, if the mode shapes in the rotary DOF can be obtained from macro-strain mode shapes, the experimental application of the rotation of mode shapes for damage detection becomes possible. Furthermore,

This study proposes the concept of utilizing mode shapes in the rotary DOF with the LFM to perform damage localization and quantification of a beam. The proposed approach only applies to change of stiffness. The macro-

---

∗Corresponding author, Assistant Professor
 E-mail: tyhsu@mail.ntust.edu.tw
[a]Professor
 E-mail: wiliao@ntut.edu.tw
[b]Research Assistant
 E-mail: 1306029@ncree.narl.org.tw

strain mode shapes are obtained by measurement of dynamic vibration signals using long-gauge FBG sensors. The mode shapes in the rotary DOF are then calculated using macro-strain mode shapes. The mode shapes in the rotary DOF and corresponding virtual load configurations are used in the LFM to detect damages of simply supported beams. Numerical studies and experimental studies are performed to verify the proposed rotary approach. The results are also compared to the approach that utilizes the LFM based on measurement of lateral vibration signals.

2. Methodology

The LFM, which not only localizes but also quantifies the damage of a structure, was developed by Reynders and De Roeck (2010) based on virtual work principle. It requires a first load system f_1 carefully chosen such that: (1) the induced stress field σ_1 can be calculated from the loading without knowledge of the structure's stiffness and (2) consists of nonzero stresses in a small local volume only. The subscript "1" represents the number of the load system. Then, it has been derived that the stiffness ratio of the local volume with nonzero stresses can be estimated using the virtual displacement x_1 induced by the first force configuration f_1 and a second force configuration f_2 that obeys the boundary condition of the system for both intact and damaged systems using

$$\frac{\sum_{j=1}^r f_{j2} x_{j1}}{\sum_{j=1}^r f_{j2} x_{j1}^d} = \frac{K + \Delta K}{K} \qquad (1)$$

where ΔK denotes the change in the stiffness parameter in the local volume due to damage. The subscript "j" represents the number of the DOF. It is assumed that ΔK remains constant within the local volume.

In the original paper, for application to a beam structure, the LFM utilizes mode shapes in the lateral DOF identified using lateral vibration signals measured with accelerometers and the corresponding virtual forces composed of lateral forces. In this study, we propose to utilize mode shapes in the rotary DOF identified using dynamic macro-strain signals measured with long-gauge FBG sensors. Accordingly, the virtual force configuration for the mode shapes in the rotary DOF should also be adjusted to be composed of moments. Consider a beam structure under the force configuration f_1 as shown in Fig. 1. Other than a lateral force, a moment is applied to the beam. If shear deformation can be neglected and the flexural rigidity (EI) remains constant between equidistant points j-1 and j+2, the force configuration of Fig. 1 causes nonzero stresses between points j-1 and j+2 only, regardless of whether the beam is isostatic or hyperstatic. This can be proved to be true if all the following three conditions are satisfied:

(1) The vector sum of all forces of Fig. 1 is zero.

(2) The resulting moment of all forces of Fig. 1 at points j-1 and j+2 is zero.

(3) The relative rotation between points j-1 and j+2, due to the force configuration, is zero.

Checking the first two conditions is trivial. The third condition can also be easily checked by means of the virtual
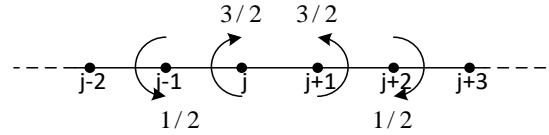

Fig. 1 A force configuration that causes virtual stresses and strains in the local region of a hyperstatic beam structure for the rotary approach. The numbers "3/2" and "1/2" are the magnitude of the components of the virtual force configuration
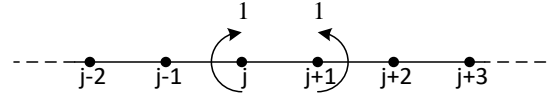

Fig. 2 A force configuration that causes virtual stresses and strains in the local region of an isostatic beam structure for the rotary approach. The numbers "1" are the magnitude of the components of the virtual force configuration

work principle by applying a virtual unit moment pair at points j-1 and j+2.

The second force configuration can be chosen as any configuration that obeys the boundary conditions. An example configuration is shown in Fig. 2.

Following Eq. (1), by applying force configuration f_1 as shown in Fig. 1 and applying force configuration f_2 as shown in Fig. 2, one can estimate rigidity ratio within the region with nonzero stress field using

$$\frac{x_j^1 - x_{j+1}^1}{x_{jd}^1 - x_{j+1,d}^1} = \frac{EI + \Delta EI}{EI} . \qquad (2)$$

It should be noted that for isostatic beams, as an alternative to the force configuration f_1 of Fig. 1, the force configuration of Fig. 2 can be applied. The proof is trivial since for isostatic structures, the relative rotation between points j and j+1 does not have to be zero in order to obtain a nonzero stress only between these points.

The displacement vector x_1 under the first load system f_1 can be obtained using the following equation

$$x_1 = H f_1 \qquad (3)$$

where H represents the flexibility matrix, which can be estimated using the identified modal parameters as follows

$$H = \sum_{r=1}^N \hat{\varphi}_r \omega_r^{-2} \hat{\varphi}_r^T \cong \sum_{r=1}^n \hat{\varphi}_r \omega_r^{-2} \hat{\varphi}_r^T \cong \sum_{r=1}^n \varphi_r \omega_r^{-2} \varphi_r^T \quad (4)$$

where $\hat{\varphi}_r$ denotes the mass-normalized mode shape of the rth mode; φ_r indicates the mode shape of the rth mode normalized to unit norm; ω_r represents the eigenfrequency of the rth mode. If only the first n modes of all the N modes are available, then the flexibility matrix is truncated. Note that contrary to the stiffness matrix, the contribution of the modes in the flexibility matrix is proportional to the inverse of the square of the eigenfrequencies. The influence of the higher modes is much smaller than that of the lower modes. As a result, the number of truncated modes needed to approximate a non-truncated flexibility matrix is much smaller than that needed to approximate a non-truncated

stiffness matrix. This benefits practical cases where only lower modes can be identified with good accuracy.

The mode shapes in the rotary DOF can be obtained by measuring the macro-strain mode shapes. By attaching a long-gauge FBG sensor onto the surface of a beam element between node j and node $j+1$, the macro-strain measured by the kth FBG sensor of gauge length l^k can be expressed as

$$\varepsilon^k = \frac{h^k}{l^k}(\theta^j - \theta^{j-1}) \tag{5}$$

where h^k represents the distance between the neutral axis of the kth FBG sensor and the neutral axis of the beam and θ^j indicates the rotary displacement at node j. Therefore, the difference in the rotary displacement between any two nodes can be obtained if the macro-strain between these two nodes is measured. Similarly, the difference in the mode shape in the rotary DOF between any two nodes can be obtained if the macro-strain mode shapes are identified from the measured macro-strain signals. The mode shape in the rotary DOF can be finally obtained if enough boundary conditions of the rotary DOF or the lateral DOF are known. For instance, the mode shape in the rotary DOF of the fixed end is zero for a cantilever beam; hence, the mode shapes in the rotary DOF at every node can be calculated. Similarly, for a simply supported beam, the relative lateral displacement of the two supports is zero if no settlement of these two supports takes place, hence the mode shapes in

the rotary DOF at every node can also be calculated using these known boundary conditions.

In this study, in order to compare the performance using the rotary approach to that from using the lateral approach, the load configuration using lateral forces in the original paper are also applied in the case studies (Reynders and De Roeck, 2010). The lateral load configuration utilized for the simply supported beam in this paper is shown in Fig. 3. Eq. (6) describes the method of estimating rigidity reduction ratios using the lateral approach.

$$\frac{-0.5x_{j-1}^1 + x_j^1 - 0.5x_{j+1}^1}{-0.5x_{j-1,d}^1 + x_{jd}^1 - 0.5x_{j+1,d}^1} = \frac{EI + \Delta EI}{EI} \tag{6}$$

The procedures of the proposed "rotary approach" and the original "lateral approach" are summarized in Fig. 4

3. Numerical studies

A numerical simply supported beam was constructed via ANSYS software to verify the proposed idea. The dimensions of the beam were 0.03 m×0.01 m×1.5 m, and the number of elements was 6, 4, and 300 along each of these respective dimensions. The element type was a three-dimensional (3D) elastic solid element with 8 nodes. The elastic modulus, the Poisson ratio, and the density of the finite element model were 2.0×10^{11} N/m^2, 0.33 and 7.8×10^3 kg/m^3, respectively. Ten long-gauge FBG sensors were designated to be installed on the bottom of the beam to monitor the beam segments labeled S1 to S10 as shown in Fig. 5. Therefore, the mode shape in the longitudinal DOF at the ends of each sensor on the bottom of the beam was utilized to calculate the macro-strain mode shapes.

Four different damage cases were considered in this study as shown in Fig. 5. The damage was simulated by reducing width of some length of a beam to consider rigidity reduction due to cracks within some range of a beam. Damage Case 1 is a symmetrical single location damage case where the width of the beam within the S5 and S6 sensor range is reduced to 20 mm. Such damage will
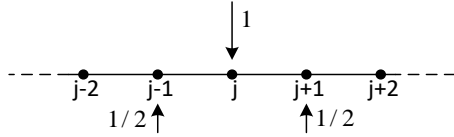
Fig. 3 A force configuration that causes virtual stresses and strains in the local region of an isostatic beam structure for the lateral approach. The numbers "1/2" and "1" are the magnitude of the components of the virtual force configuration
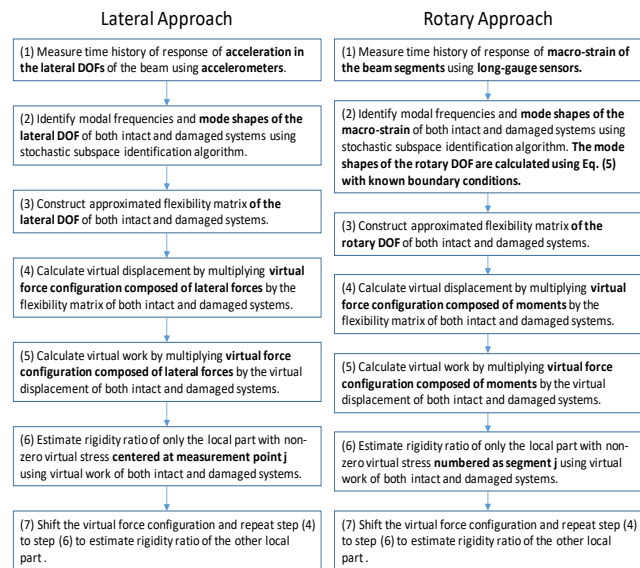
Fig. 4 A procedure diagram of both the proposed "rotary approach" and the original "lateral approach"
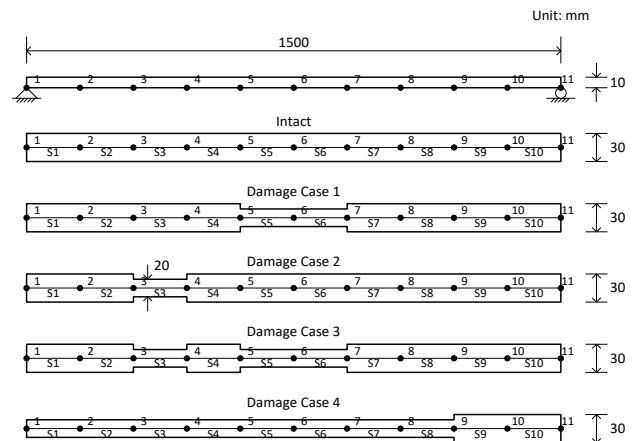
Fig. 5 A simply supported beam model for numerical studies. The first figure is the side view of the beam. The other five figures below are the top views of the beam

cause 33.3% of flexural stiffness reduction of the damaged beam segments; Damage Case 2 is an unsymmetrical single damage case where the width within the S3 range is reduced to 20 mm; Damage Case 3 is a multi-damage-location case mixed by the first 2 damage cases; and Damage Case 4 is a continuous damage case where the width within the S1 to S8 range is reduced to 20 mm. Note that if no change in stiffness is present, the rigidity ratio will be estimated as close to 1.0.

The flexibility matrices of different cases were calculated utilizing the mode shapes in the rotary DOF and the natural frequencies obtained from the numerical model. In practice, the number of qualified fundamental modes identified from measured vibration signals is limited. Therefore, in this study, the numbers of the lowest fundamental modes n considered were 1, 2, 3, 5, and 10 in order to view the effects on damage detection results caused by the truncation of modes when constructing the flexibility matrices. For each segment, the force configuration of Fig. 2 was utilized as both the first load configuration f_1 and the second load configuration f_2. The flexural rigidity ratios $(EI+\Delta EI)/EI$ at every segment of the different damage cases utilizing different numbers of modes as well as the designated flexural rigidity ratios for reference are illustrated in Fig. 6.
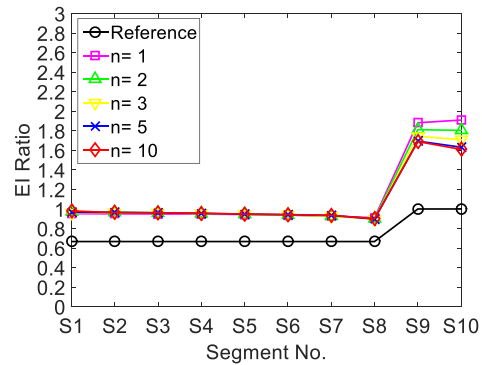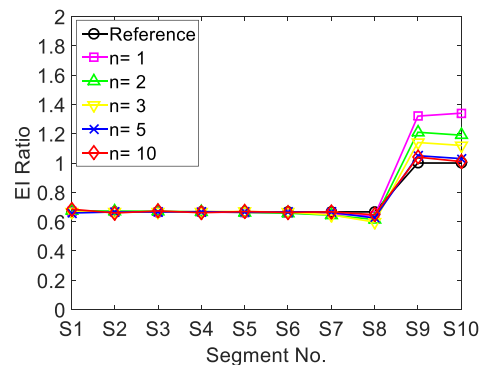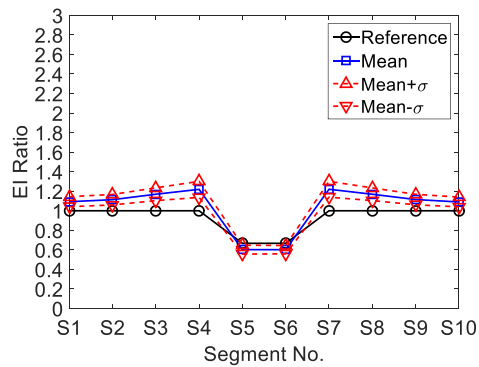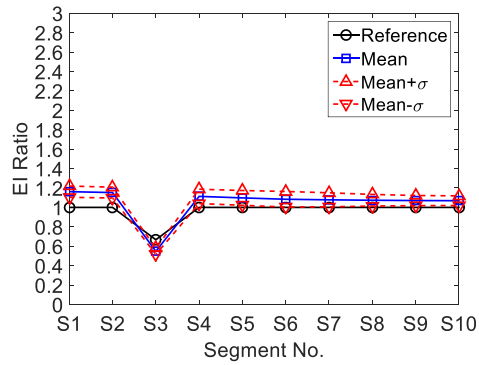

(a)

(b)
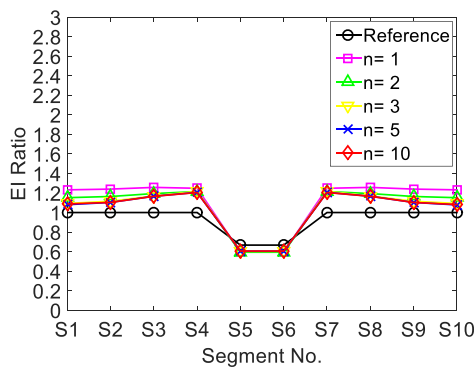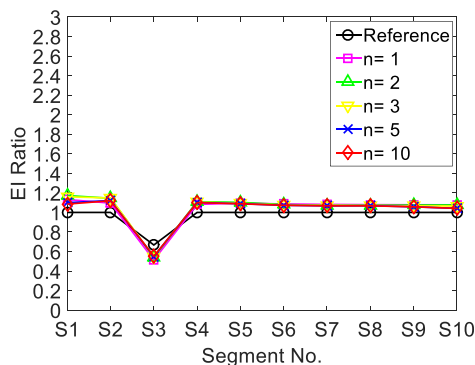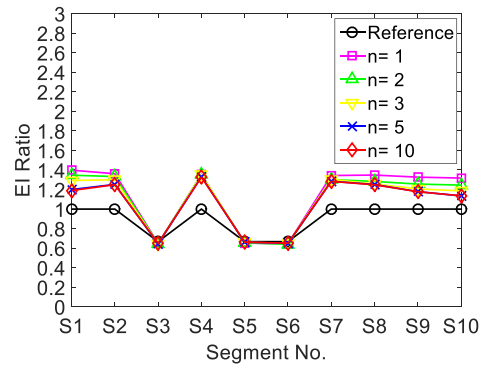
Fig. 6 Estimated flexural rigidity ratio utilizing a different number of non-mass-normalized modes for (a) Damage Case 1; (b) Damage Case 2; (c) Damage Case 3; (d) Damage Case 4; and (e) the mass-normalized modes for Damage Case 4


(c)

(d)

(e)

Fig. 6 Continued

It can be seen from Fig. 6 that, in general, the flexural rigidity ratios estimated utilizing the first few modes can not only locate the damage locations but can also quantify the damage with an acceptable accuracy, except for Damage Case 4. It is worth noting that even if only the first mode was utilized, the flexural rigidity ratios within the damage zones were estimated quite close to the reference value for the first three damage cases. The methodology seems effective for either symmetrical or unsymmetrical damage or single/multiple damage cases. For Damage Case 4 where most of the segments are damaged continuously, the extents of estimated rigidity ratio of the damaged segments are close to 1.0 while those of the intact segments are much higher than 1.0. In this continuously damaged case, although the error of the damage extent is large, the damage locations may still be observed since the change in the
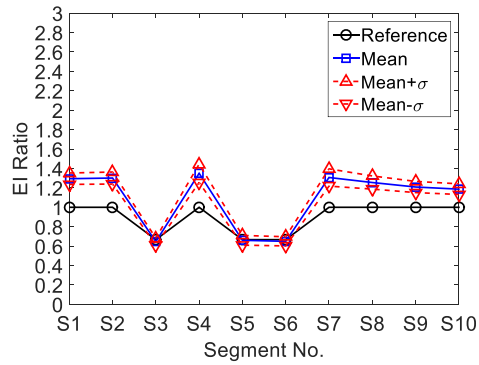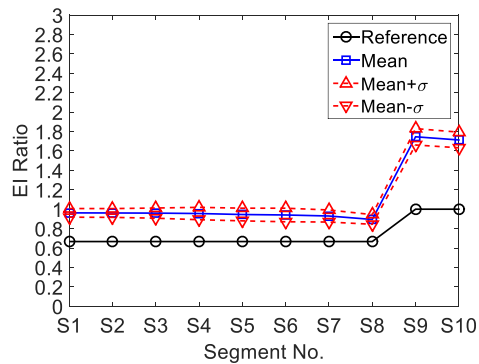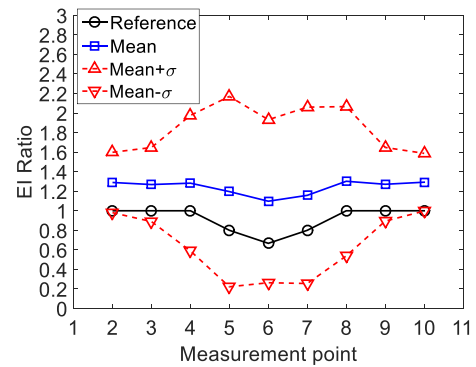
Fig. 7 Estimated flexural rigidity ratio utilizing the first three modal parameters with a 2% noise level using the rotary approach for different damage cases: (a) Damage Case 1; (b) Damage Case 2; (c) Damage Case 3; and (d) Damage Case 4
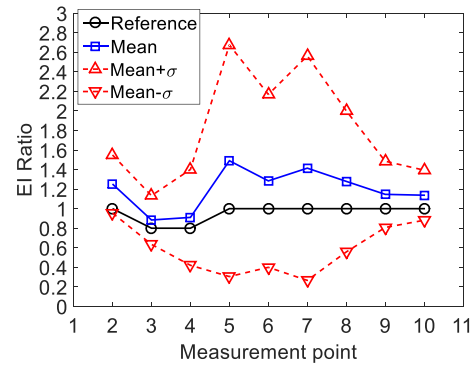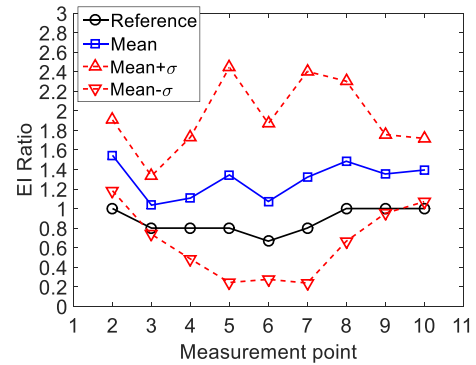
Fig. 8 Estimated flexural rigidity ratio utilizing the first three modal parameters with a 2% noise level using the lateral approach for different damage cases: (a) Damage Case 1; (b) Damage Case 2; (c) Damage Case 3; and (d) Damage Case 4
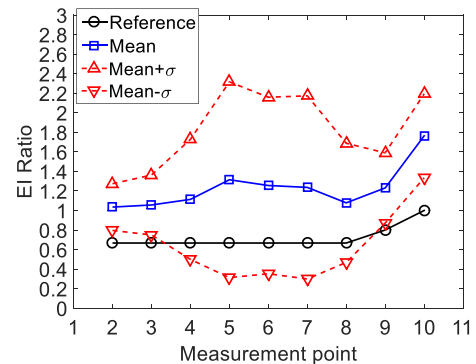
rigidity ratios is large and the difference between the intact and damaged segments is also great. In other words, when the abnormally high rigidity ratios of only some segments are observed, it is probably not the increase of rigidity of these segments with abnormally high rigidity ratios but rather the decrease of rigidity of the other segments. The estimated error is possibly due to the approximation of the flexibility matrix using non-mass-normalized mode shapes. If the mass-normalized mode shapes were used to estimate the flexibility matrix, then the error becomes much smaller as shown in Fig. 6(e).

The natural frequencies and mode shapes identified from the measured vibration signals may contain errors and the flexibility matrix is constructed utilizing these modal parameters. Therefore, the estimated flexural rigidity ratio could be altered by these errors in the identified modal parameters. In this study, the noise effect of the modal parameters was investigated. Random noise of Gaussian distribution with a standard deviation of 2% was added directly to the natural frequencies and the macro-strain mode shapes for both the intact and damaged cases. That is, the magnitude of the standard deviation of the added random noise was 2% of the magnitude of the original parameters. The first three lowest fundamental modes were utilized to construct the flexibility matrix (i.e., $n=3$), which is realistic for most of the practical cases. The flexural rigidity ratio was estimated 1000 times for each case and then the mean and standard deviation of the estimated flexural rigidity ratio were calculated. Fig. 7(a) to 7(d) illustrate the estimated flexural rigidity ratio of the four damage cases considering noise effects. It can be observed that although the 2% noise level induced some estimation error, damage localization and quantification was still quite successful. Moreover, the standard deviation of the error caused by the noise at the damaged segments is slightly smaller than the one at the intact segments.

In addition, random noise of Gaussian distribution with a noise level with a standard deviation of 2% was added directly to the natural frequencies and mode shapes in the lateral DOF for both the intact and damaged cases. The mode shapes were assumed to be measured at the eleven nodes as shown in Fig. 5. Similar to the original paper, the load configuration as shown in Fig. 3 was used as both the first and second load configurations. The flexural rigidity ratio was estimated using the first three lowest fundamental modes 1000 times. In Fig. 8, the estimated flexural rigidity ratio at each measurement point represents the estimated rigidity ratio using the load configuration centered at each corresponding measurement point. The mean and standard deviation of the estimated flexural rigidity ratio at each measurement point were calculated and are shown in Fig. 8 for the same four damage cases. It is evident that the effect of noise increases the difficulty in damage localization and quantification. Note that the error caused by the 2% noise level in the displacement mode shapes in the lateral DOF is much higher than the one caused by the 2% noise level in the macro-strain mode shapes.

4. Experimental studies

For the traditional LFM using lateral measurements such as acceleration responses of a beam element, in order to ensure that the stress induced by virtual forces only exists within a local region, the distance of each successive section of the beam element must be identical. This becomes a restriction for employing the LFM. On the other hand, based on the methodology derived in the previous section, a potential merit of the proposed approach using the macro-strain measurement is that the distance between each pair of joints can be different. This release of the restriction of equal distance between adjacent measurement joints could benefit the damage detection of beam structures using the LFM since the setup of macro-strain measurements can be easily adjusted according to demand. For example, for a cantilever beam structure, the beam elements that experience the largest moment are the ones that are close to the fixed end if a concerned lateral load is applied at the free end of the beam. Hence, these elements may deserve a denser arrangement of sensors for health monitoring under this load pattern during operation. Another example is that if more attention is desired for certain beam elements (for e.g., the elements that are close to the support of a simply supported beam), the sensor can also be arranged to be concentrated on that region. For the other beam elements that are of lower concern, fewer sensors can be arranged to be installed within these elements to reduce effort and cost of both installation and maintenance for structural health monitoring.

Since this paper aims to prove the feasibility of the proposed new approach using rotary DOF with macro-strain measurement, unlike the numerical study, only limited number of sensors were employed in this experimental study. The number of long-gauge sensors was determined by the length of available shortest commercial long-gauge macro sensors and the length of the beam. A simply supported steel beam with dimensions 0.05 m×0.008 m×1.95 m was constructed as shown in Fig. 9. The shortest length of the packaged long-gauge FBG sensor was 40 cm, which means only a few long-gauge FBG sensors could be installed onto the beam specimen within the limited length. In order to demonstrate the ability of length customization of the long-gauge FBG sensors, two different lengths of the long-gauge
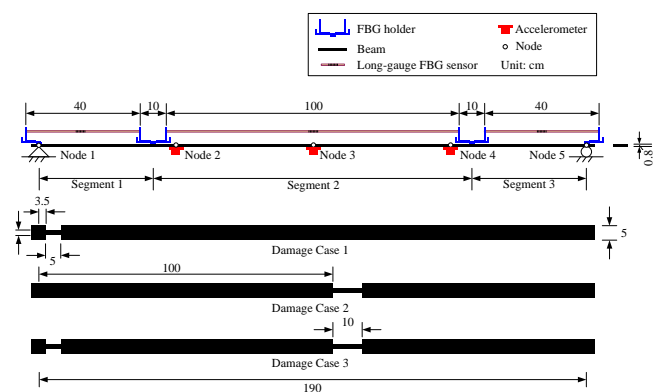

Fig. 9 A simply supported beam specimen for experimental studies. The first figure is the side view of the whole setup of the beam specimen. The other three figures below are the top views of the steel beam
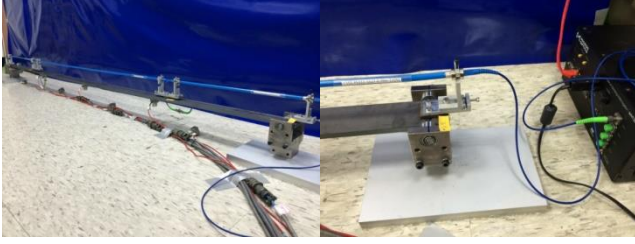
Fig. 10 A simply supported beam specimen with long-gauge FBG sensors and accelerometers: overview (left); and close view (right)
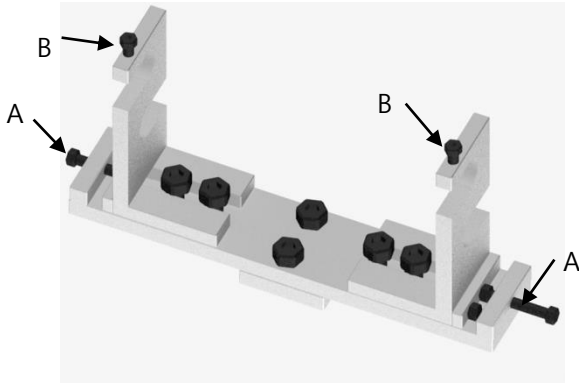

Fig. 11 A schematic diagram of a typical long-gauge FBG holder

FBG sensors were employed. As a results, totally only two 40 cm long-gauge FBG sensors and one 100 cm long-gauge FBG sensor were installed. Although high modes of the beam will be difficult to be identified using only these three long-gauge sensors, actually, only the first mode can be enough to construct a flexibility matrix with acceptable accuracy to estimate rigidity ratios using LFM as illustrated in the original paper (Reynders and De Roeck 2010). This is the merit of LFM because a monitoring system with dense FBG sensors are costly mainly because expensive sensing interrogators are required. Although more sensors usually lead to better damage identification results, a monitoring system with less FBG sensors is more practical in the financial aspect when acceptable damage identification results can be obtained.

These FBG sensors composed of thin plastic tube and slim optical fiber in the core were connected in series to the MOI SI-425 sensing interrogator. To achieve the same density of the accelerometers, three Setra141 accelerometers were attached to the bottom of the beam and the vertical acceleration response was recorded by the NI-9205 data acquisition module. Note that these accelerometers had to be installed with equal spacing if the mode shapes in the lateral DOF were used. Because an interval between the ends of each long-gauge FBG sensor was required to connect each sensor, the long-gauge FBG holder made by aluminum was designed as shown in Fig. 10 and Fig. 11. The screws "A" of the holders were designed to provide small pre-tension of the FBG sensors so that the both compression and tension vibrating signals of the FBG sensors could be measured, while the screws "B" was for fixing after screws "A" was set. The holder was

attached to the steel beam only via a small steel patch. Because the Young's modulus and dimension of the FBG sensor was much smaller than the ones of the beam specimen, the flexural stiffness contribution of the FBG sensor was actually less than 5% and hence can be neglected. Besides, since the stiffness of the aluminum holder was much higher than the stiffness of the long-gauge FBG sensor, the holder showed similar behavior to a rigid body when the beam was vibrating. As a result, the measured dynamic macro-strain signals of the long-gauge FBG sensors were mainly contributed from the flexural deformation of the beam.

The macro-strain mode shapes identified from the dynamic macro-strain signals could be used to calculate the mode shape in the rotary DOF using the following equation

$$\frac{\gamma_i^k l^k}{h^k} = (\varphi_i^k - \varphi_i^{k-1}) \tag{7}$$

where γ_i^k is the macro-strain mode shape of the ith mode of the kth long-gauge FBG sensor; and l^k represents the length of the kth long-gauge FBG sensor. The distance between the central axis of the sensors and the central axis of the beam was 60 mm. For this simply supported beam, as the relative lateral displacement of the two supports was zero since no settlement of these two supports took place, the initial mode shapes in the rotary DOF at the boundaries could be easily estimated.

Three different damage cases were considered in this study as shown in Fig. 9. Damage Case 1 simulates a single damage close to the left support where the width of the damaged range with a length of 50 mm is reduced to 20 mm. Such damage will cause 60% of flexural stiffness reduction of the beam element within the 50 mm range. Damage Case 2 simulates another single damage close to the middle of the beam where the width of the damaged range with a length of 100 mm is reduced to 20 mm. Such damage will cause 60% of flexural stiffness reduction of the beam element within the 100 mm range. Finally, Damage Case 3 is a multi-damage-location case mixed by the first 2 damage cases.

As the size of the beam specimen was quite small, the beam was excited by impact forces simulated by a human finger tapping at several different points. For each test, both the vertical acceleration at node 2 to node 4 and macro-strain vibration signals of the three long-gauge FBG sensors were collected for 60 seconds at a sampling rate of 250 Hz. The modal parameters, i.e., modal frequencies, modal damping and mode shapes, were identified from the output-only acceleration measurement or macro-strain measurement using the stochastic subspace identification algorithm (Van Overschee and De Moor 1996). The rigidity ratio was estimated following similar procedure in the numerical study using these identified modal parameters and the same virtual forces as in the numerical studies. The reference value of the rigidity ratio was calculated using the corresponding virtual force configurations and the flexibility matrix constructed using modal parameters obtained from finite element beam models. Note that the DOFs of the mode shapes of "rotary approach" and "lateral

approach" were different. The virtual force configurations of these two approaches were also different. Therefore, the reference value of these two approaches were different. Besides, the holders were considered in the finite element model constructed using ANSYS software and the effect of mass and stiffness of the holder was found very small, as can be observed in the reference value of rigidity ratios in Fig. 12 to Fig. 14.

In Fig. 12(a), the estimated and reference rigidity ratio of the first damage case using the modal parameters in the lateral DOF are plotted. Since the damage location is between node 1 and node 3, the reference value at measurement point 2, which represents the rigidity ratio between these regions, is expected to be less than 1.0. However, observation of the reference value indicates that theoretically it is not easy to detect the damage close to the support in this case since the reference value at measurement point 2 almost equals 1.0. Moreover, the error of the estimated rigidity ratio using the modal parameters in the lateral DOF may make the damage localization and quantification results quite confusing, especially for the case using only the first mode. On the other hand, the reference rigidity ratio at the 1st segment is 0.83 in Fig. 12(b) using the mode shapes in the rotary DOF. The estimated rigidity ratio using the first modal parameters in the rotary DOF clearly identifies the damage location at the first segment with acceptable estimation of the damage extent. However, the error of the estimated rigidity ratios using the first two modal parameters in the rotary DOF becomes even larger at both the first segment and the third segment.

For the second damage case, the estimated and reference rigidity ratio using the modal parameters in the lateral DOF are shown in Fig. 13(a). The reference value indicates that the theoretical value at measurement point 2 approximates to 0.79, while the one at measurement point 3 approximates to 0.96. The estimated rigidity ratios using the first modal parameters in the lateral DOF are quite close to the

reference value at these two points. However, the error of the estimated rigidity ratio using the first two modal parameters in the lateral DOF becomes even larger. On the other hand, the estimated and reference rigidity ratio using the modal parameters in the rotary DOF are shown in Fig. 13(b). The reference value indicates that the theoretical value at measurement point 2 approximates to 0.87. The estimated rigidity ratio using the first rotary modal parameters is quite close to the reference value at this point. The estimated rigidity ratio using the first two modal parameters in the rotary DOF is also quite close to the reference value at this point. However, the error of the estimated rigidity ratios using the first two modal parameters in the rotary DOF is even smaller at the other points compared to the ones using only the first modal parameters in this case.

For the third damage case with a mixed damage of the first two damage cases, the reference value and estimated value of the rigidity ratios using modal parameters in the lateral DOF and in the rotary DOF are shown in Fig. 14(a) and Fig. 14(b), respectively. It is evident that the error of the estimated rigidity ratios using the modal parameters in the lateral DOF is quite large; thus, damage localization is somewhat difficult. On the other hand, the estimated rigidity ratios using the modal parameters in the rotary DOF are much more acceptable. The two damage locations are clearly identified with an acceptable damage extent estimation using the first modal parameters in the rotary DOF. However, the error of the estimated rigidity ratio at the first segment increases if the first two modal parameters in the rotary DOF are used. The values of the rigidity ratios using the "lateral approach" and the "rotary approach" in Fig. 12 to Fig. 14 are summarized in Table 1 and Table 2, respectively.

The holder of the long-gauge FBG sensor is designed to have less effect on the beam (i.e., less weight, higher stiffness comparing to the long-gauge FBG sensor, and attached to the beam via a small point). In practical, for such a small holder installed in a real bridge, no effects are
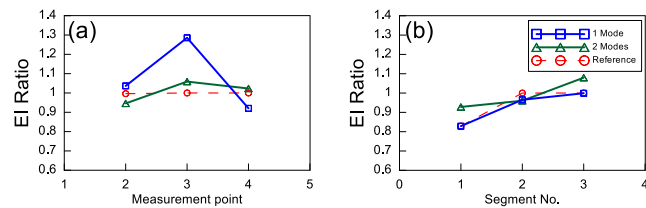

Fig. 12 Estimated rigidity ratio for the first damage case using the (a) modal parameters in the lateral DOF; and (b) modal parameters in the rotary DOF
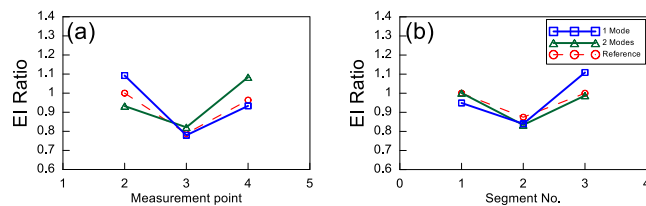

Fig. 13 Estimated rigidity ratio for the second damage case using the (a) modal parameters in the lateral DOF; and (b) modal parameters in the rotary DOF
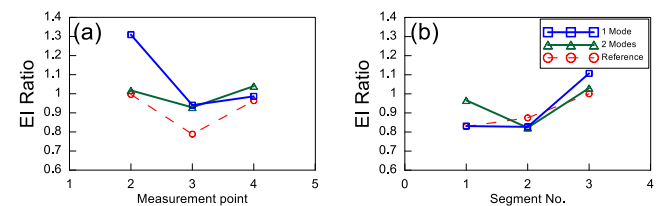

Fig. 14 Estimated rigidity ratio for the third damage case using the (a) modal parameters in the lateral DOF; and (b) modal parameters in the rotary DOF

Table 1 The rigidity ratios using the "lateral approach" in Fig. 12 to Fig. 14

Measurement point	Case 1			Case 2			Case 3		
	1 Mode	2 Modes	Reference	1 Mode	2 Modes	Reference	1 Mode	2 Modes	Reference
2	1.04	0.95	1.00	1.09	0.93	1.00	1.31	1.02	1.00
3	1.29	1.06	1.00	0.78	0.82	0.79	0.94	0.93	0.79
4	0.92	1.02	1.00	0.93	1.08	0.96	0.99	1.04	0.96

Table 2 The rigidity ratios using the "rotary approach" in Fig. 12 to Fig. 14

Segment point	Case 1			Case 2			Case 3		
	1 Mode	2 Modes	Reference	1 Mode	2 Modes	Reference	1 Mode	2 Modes	Reference
1	0.83	0.93	0.83	0.95	1.00	1.00	0.83	0.97	0.83
2	0.97	0.96	1.00	0.84	0.83	0.87	0.83	0.82	0.87
3	1.00	1.08	1.00	1.11	0.99	1.00	1.11	1.03	1.00

required to be considered because the mass, stiffness, and size are very small comparing to a real bridge. Actually, these holders are already considered in the finite element model constructed using ANSYS software and the effect of mass and stiffness of the holder is very small, as can be observed in the reference value of EI ratios in Fig. 12 to Fig. 14.

Based on the comparison of the estimated rigidity ratios of these three damage cases using the modal parameters in the lateral DOF and in the rotary DOF, in general, the damage locations are identified more clearly and the estimated damage extents are closer to the reference values using the modal parameters in the rotary DOF with the LFM. In fact, the local region with a non-zero stress using the rotary approach is smaller than the one using the lateral approach. For the lateral approach, the local region is between three nodes whereas the local region for the rotary approach is only between two. Since only the average rigidity ratio can be estimated within the local region, the same extent of damage induces a higher reduction ratio if a smaller local region is valid. That is, the rotary approach is more sensitive to damage, especially when the size or extent of the damage is smaller. Furthermore, if the virtual forces of the lateral approach are used, the induced moment closer to the center of the virtual forces is higher than the one at the other parts in the local region. Therefore, when the damage is not close to the center of the local region, the average reduction ratio will be very small. As a result, when the damage is closer to a support, it is not easily detected using the lateral approach. On the other hand, since the induced moment is uniform within a local region if the virtual forces of the rotary approach are used, it is still possible to identify damage even if it is very close to the support.

5. Conclusions

This study proposes the new concept of utilizing macro-strain measurements via the Local Flexibility Method (LFM) to perform damage localization and quantification of a beam structure. The macro-strain mode shapes are obtained by the measurement of dynamic vibration signals using long-gauge Fiber Bragg grating (FBG) sensors and then the mode shapes in a rotary degree of freedom (DOF) are calculated using the macro-strain measurements. The mode shapes in the rotary DOF and the eigenfrequencies are used to estimate the flexibility matrices of a beam structure both before and after damage. Based on the LFM

algorithm and the modified visual force configurations, the location and extent of the damage of beam segments can be estimated. Note that compared to static measurement using FBG sensors whose signals may be significantly affected by temperature, the signals of dynamic vibration signals of FBG sensors may not be directly affected by temperature and are mainly correlated to the properties of the structure, e.g., the rigidity.

The results of the proposed rotary approach were compared to those obtained using the traditional lateral approach via both numerical and experimental studies. From the numerical studies, it was found that the rotary approach is more robust to noise in the measurement if the same level of noise exists in the modal parameters. However, note that in real applications, the noise level of macro-strain mode shapes and displacement mode shapes in the lateral DOF depends on the measurement methodology and measurement conditions. The noise level of these two measurements could be quite different, which is beyond the scope of this study. From the experimental studies it was found that the proposed rotary approach has two other advantages. The first advantage is that the sensor configuration can be flexible. That is, the length of the long-gauge FBG sensor can be different for each adjacent segment. Therefore, sensor deployment can be customized for different applications and hence a more cost-effective arrangement of sensors could be achieved. Furthermore, when the damage is close to the supports of a simply supported beam, the damage is more likely to be discovered using the rotary approach, outlining another significant advantage of using the proposed method.

Acknowledgments

References

Abdo, M.A.B. and Hori, M. (2002), "A numerical study of structural damage detection using changes in the rotation of mode shapes", *J. Sound Vib.*, **251**(2), 227-239.

Ansari, F. (2005), "Fiber optic health monitoring of civil structures using long gage and acoustic sensors", *Smart Mater. Struct.*, **14**(3), S1.

Bernal, D. (2002), "Load vectors for damage localization", *J. Eng. Mech.*, **128**(1), 7-14.

Cardini, A.J. and DeWolf, J.T. (2009), "Long-term structural health monitoring of a multigirder steel composite bridge using strain data", *Struct. Hlth. Monit.*, **8**(1), 47-58.

Fan, N.Y., Huang, S. and Measures, R.M. (1998), "Localized long gage fiber optic strain sensors", *Smart Mater. Struct.*, **7**(2), 257.

Johnson, E., Lam, H., Katafygiotis, L. and Beck, J. (2004), "Phase I IASC-ASCE structural health monitoring benchmark problem using simulated data", *J. Eng. Mech.*, **130**(1), 3-15.

Li, S.Z. and Wu, Z.S. (2007), "Development of distributed long gage fiber optic sensing system for structural health monitoring", *Struct. Hlth. Monit.*, **6**(6), 133-143.

Li, S.Z. and Wu, Z.S. (2010), "Parametric estimation for RC flexural members based on distributed long- gauge fiber optic

sensors", *J. Struct. Eng.*, **136**(2), 144-151.

Matthys, S. and Taerwe, L. (2005), "Experimental testing of posttensioned concrete girders instrumented with optical fiber gratings", *Proceeding of the SPIE-17th International Conference on Optical Fiber Sensors*, SPIE, Bellingham, Wash., 1060-1063.

Ni, Y., Xia, H., Wong, K. and Ko, J. (2012), "In-service condition assessment of bridge deck using long-term monitoring data of strain response", *J. Bridge Eng.*, **17**(6), 876-885.

Reynders, E. and De Roeck, G. (2010), "A local flexibility method for vibration-based damage localization and quantification", *J. Sound Vib.*, **329**(12), 2367-2383.

Toksoy, T. and Aktan, A.E. (1994), "Bridge-condition assessment by modal flexibility", *Exp. Mech.*, **34**(3), 271-278.

Van Overschee, P. and De Moor, B. (1996), *Subspace Identification for Linear Systems: Theory - Implementation - Applications*, Kluwer Academic Publishers: Dordrecht, The Netherlands.

Yung, B.L., Chang, K.C., Chern, J.C. and Wang, L.A. (2004), "The health monitoring of a prestressed concrete beam by using fiber Bragg grating sensors", *Smart Mater. Struct.*, **13**(4), 712-718.

Wan, L.B., Wu, Z.J., Zhang, B.M., Wang, D.F., Zhao, X. and Zhou, Z. (2002). "Determination of internal strain of concrete beam using fiber Bragg grating sensors", *J. Optoelectron. Laser*, **13**(7), 722-725.

Wang, M.L. and Yim, J. (2010), "Sensor enriched infrastructure system", *Smart Struct. Syst.*, **6**(3), 309-333.

Wang, L., Han, J. and Song, Y. (2014), "Fatigue performance monitoring of full-scale PPC beams by using the FBG sensors", *Smart Struct. Syst.*, **13**(6), 943-957.

BS